J|A|C|S
ARTICLES
Published on Web 07/13/2006

Wheel-Shaped Polyoxotungstate $[Cu_{20}Cl(OH)_{24}(H_2O)_{12}(P_8W_{48}O_{184})]^{25-}$ Macroanions Form Supramolecular "Blackberry" Structure in Aqueous Solution

Guang Liu,[†] Tianbo Liu,*[,†] Sib Sankar Mal,[‡] and Ulrich Kortz[‡]

Contribution from the Department of Chemistry, Lehigh University, Bethlehem, Pennsylvania 18015, and School of Engineering and Science, International University Bremen, P.O. Box 750 561, 28725 Bremen, Germany

Received February 14, 2006; E-mail: til204@lehigh.edu

Abstract: The hydrophilic polyoxotungstate $[Cu_{20}Cl(OH)_{24}(H_2O)_{12}(P_8W_{48}O_{184})]^{25-}$ ($\{Cu_{20}P_8W_{48}\}$) self-assembles into single-layer, hollow, spherical "blackberry"-type structures in aqueous solutions, as studied by dynamic light scattering (DLS), static light scattering (SLS), zeta potential analysis, and scanning electron microscopy (SEM) techniques. This represents the first report of blackberry formation for a non-Mo-containing polyoxometalate. There is no obvious change in the shape and size of the blackberries during the slow blackberry formation process, neither with macroionic concentration nor with temperature. Our results suggest that the blackberry-type structure formation is most likely a general phenomenon for hydrophilic macroions with suitable size and charge in a polar solvent, and not a specific property of polyoxomolybdates and their derivatives. The $\{Cu_{20}P_8W_{48}\}$ macroions are thus far the smallest type of macroions to date (equivalent radius < 2 nm) showing the unique self-assembly behavior, helping us to move one step closer toward identifying the transition point from simple ions (can be described by the Debye−Hückel theory) to macroions in very dilute solutions. Moreover, by using $\{Cu_{20}P_8W_{48}\}$ blackberry-type structures as the model system, the electrophoretic properties of macroionic supramolecular structures are studied for the first time via zeta-potential analysis. The mobility of blackberry-type structures is determined and used for understanding the state of small cations in solution. We notice that the average charge density on each $\{Cu_{20}P_8W_{48}\}$ macroanion in a blackberry is much lower than that of discrete "free" $\{Cu_{20}P_8W_{48}\}$ macroions. This result suggests that some small alkali counterions are closely associated with, or even incorporated into, the blackberry-type structures and thus do not contribute to solution conductivity. This model is fully consistent with our speculation that monovalent counterions play an important role in the self-assembly of macroions, possibly providing an attractive force contributing to blackberry formation.

Introduction

Polyoxometalates (POMs) represent a large group of early transition metal−oxygen anionic clusters with enormously diverse chemical structures, physical properties, and promising applications as catalytic, magnetic, electrical, and optical materials.[1−3] Due to their highly negative charge and water ligands on the surface, most POMs are hydrophilic and highly soluble in polar solvents. Recent discoveries demonstrate that some giant polyoxomolybdates (so-called POM macroions, with diameters of several nanometers) exhibit fascinating solution behaviors. Unlike common soluble electrolytes that disperse homogeneously in aqueous solutions, such highly soluble macroions tend to further self-associate into spherical, single-layer, vesicle-like, "blackberry"-type structures in very dilute solutions. These observations have introduced fundamentally novel aspects to POM chemistry in particular and also to solution physical chemistry in general.[4−12] The blackberry-type structure formation differs from the aggregation of hydrophobic colloids (due to van der Waals forces) which leads to phase separation. On the other hand, the macroionic solutions are transparent and thermodynamically stable, without any phase separation. Thermodynamic studies indicate that the macroionic solution is a novel type of solution state which differs from simple ionic solutions. To overcome the electrostatic repulsion between negatively charged macroions, certain driving forces must be present when the macroions move closer to each other

[†] Lehigh University.
[‡] International University Bremen.

(1) Pope, M. T. *Heteropoly and Isopoly Oxometalates*; Springer-Verlag: New York, 1983.
(2) Hill, C. L., Ed. Polyoxometalates. *Chem. Rev.* **1998**, *98*, 1−387.
(3) Yamase, T.; Pope, M. T. Eds. *Polyoxometalate Chemistry for Nano-Composite Design*; Kluwer Academic/Plenum Publishers: New York, **2002**, 1−227.
(4) Müller, A.; Diemann, E.; Kuhlmann, C.; Eimer, W.; Serain, C.; Tak, T.; Knöchel, A.; Pranzas, P. K. *Chem. Commun.* **2001**, *19*, 1928.
(5) Liu, T. *J. Am. Chem. Soc.* **2002**, *124*, 10942; *J. Am. Chem. Soc.* **2004**, *126*, 406 (Addition/Correction).
(6) Liu, T. *J. Am. Chem. Soc.* **2003**, *125*, 312.
(7) Liu, T.; Diemann, E.; Li, H.; Dress, A.; Müller, A. *Nature* **2003**, *426*, 59.
(8) Liu, G.; Cai, Y.; Liu, T. *J. Am. Chem. Soc.* **2004**, *126*, 16690.
(9) Liu, G.; Liu, T. *J. Am. Chem. Soc.* **2005**, *127*, 6942.
(10) Liu, G.; Liu, T. *Langmuir* **2005**, *21*, 2713.
(11) Zhu, Y.; Cammers-Goodwin, A.; Zhao, B.; Dozier, A.; Dickey, E. C. *Chem. Eur. J.* **2004**, *10*, 2041.
(12) Chen, B.; Jiang H.; Zhu, Y.; Cammers, A.; Selegue, J. P. *J. Am. Chem. Soc.* **2005**, *127*, 4166.

during the blackberry-type structure formation. The driving forces behind the self-assembly of macroions are not caused by hydrophobic interaction (responsible for the surfactant micelle formation) because there is no hydrophobic part in POM macroions, or van der Waals forces (responsible for the aggregation of colloids), as we have proven previously.[9] We have found that the presence of charges on POM clusters is necessary for the blackberry-type structure formation, and therefore, the counterion effect plays an important role.[9]

Many important issues regarding the blackberry-type structures remain still unclear. For example, blackberry formation has been observed for several types of large POMs, but the critical size limit at which the simple ions will behave like macroions and generate strong attractive forces between them is still unknown. The popular Debye−Hückel theory is widely used for understanding dilute solutions of low-valent (ideally 1:1) electrolytes. However, POM solutions might be more complicated since POM macroanions are large. The disparity between the sizes and charge densities of POM macroions and small cations appears to be responsible for the "counterion association" phenomenon which we have observed recently for some giant, multi-nanometer-size POM solutions, e.g. $[As_{12}Ce_{16}(H_2O)_{36}W_{148}O_{524}]^{76-}$ ($\{W_{148}\}$)[13] and $[\{Mo_{72}O_{252}(H_2O)_{72}\}\cdot\{Mo_2O_4(CH_3COOH)\}_{30}]^{42-}$ ($\{Mo_{132}\}$).[14,15] On the other hand, previous reports show that the Debye−Hückel theory is applicable to some smaller POM ionic solutions, such as $[PMo_{12}O_{40}]^{n-}$ [16] and $[SiVW_{11}O_{40}]^{n-}$ [17] (equivalent size <1 nm for both types of ions). Until now, all the observed blackberry formations are related to giant Mo-containing polyoxometalate clusters (at least 2.5-nm in diameter), such as $\{Mo_{132}\}$[11−12,14], $[Mo_{72}Fe_{30}O_{252}(CH_3COO)_{12}\{Mo_2O_7(H_2O)\}_2\{H_2Mo_2O_8(H_2O)\}(H_2O)_{91}](\{Mo_{72}Fe_{30}\})$[5−6,8−10,18], $\{[Mo_{154}O_{462}H_{14}(H_2O)_{70}]_{0.5}[Mo_{152}O_{457}H_{14}(H_2O)_{68}]_{0.5}\}^{15-}$ ($\{Mo_{154}\}$)[4,7,19], $[Mo_{176}O_{528}H_{16}(H_2O)_{80}]^{16-}$ ($\{Mo_{176}\}$)[20,21], etc. We speculate that the blackberry formation and the association of counterions to POM macroions might be correlated. The fact that macroions self-assemble into supramolecular structures may indicate that the Debye−Hückel theory is not applicable for explaining the complicated solution behavior of POM macroions. Therefore, it appears important to explore the transition point from simple ions to macroions, i.e., at what size limit do the soluble inorganic ions start to exhibit totally different solution behavior (e.g., blackberry formation).

A second important question is whether the blackberry formation is a general type of phenomenon for macroions, or a specific feature of Mo-containing macroions. We tend to believe the former, but it is also a fact that until now all blackberry formations were observed for polyoxomolybdates and their derivatives. Do they perhaps possess unique structural or electronic features resulting in unique self-assembly behavior in solution different from polyoxotungstates and polyoxovanadates? To clarify this point, we decided to expand our studies to polyoxotungstates.

Finally, we have shown that the charges on macroions play a decisive role in the self-assembly of macroions.[9] Previously, we mentioned that there are two different types of charges on POM macroions: delocalized charges (e.g., in $\{Mo_{154}\}$ and $\{Mo_{368}\}$) and localized charges (e.g., $\{Mo_{72}Fe_{30}\}$. When the macroions are uncharged (neutral molecules), they stay as discrete clusters stably in solution. However, they tend to form blackberry-type structures by strongly attracting each other when they carry charges, in spite of the fact that they become more soluble with increasing negative charges.[9] This result clearly indicates that the presence of charges on POMs is critical for the self-assembly of macroions, and in fact the large blackberry structures are also highly negatively charged. However, until now there is no study of the electrophoretic properties of the blackberry-type structures, and the role of small counterions in blackberry-type structure formation and structure is also not yet understood. The key question here is whether the counterions are involved in the blackberry-type structure formation by providing an attractive force between two adjacent macroions (so-called like-charge attraction). First, we need to confirm whether the counterions are closely associated with blackberry-type structures in solution, or if they stay essentially as free ions in solution.

To answer the above three key questions, we have conducted research on the aqueous solutions of the wheel-shaped, copper-containing tungstophosphate, $[Cu_{20}Cl(OH)_{24}(H_2O)_{12}(P_8W_{48}O_{184})]^{25-}$ ($\{Cu_{20}P_8W_{48}\}$).[22] Unlike some of Müller's polyoxomolybdates, all atoms in $\{Cu_{20}P_8W_{48}\}$ are in well-defined oxidation states and there are no delocalized electrons. Furthermore, $\{Cu_{20}P_8W_{48}\}$ is smaller in size (2 nm × 2 nm × 1 nm) than the above-mentioned Mo-containing POMs showing blackberry formation. The $\{Cu_{20}P_8W_{48}\}$ clusters are thermally and oxidatively stable in solution (compared to some Mo^V-containing clusters which tend to be oxidized slowly in solution). These favorable properties of $\{Cu_{20}P_8W_{48}\}$ enable us to perform more detailed, quantitative studies on its solution behaviors, especially the electrophoretic properties, by using zeta potential analysis.

Experimental Section

1. Sample Preparation. The $\{Cu_{20}P_8W_{48}\}$ macroion has a wheel-shaped structure with a diameter of ~2.0 nm and a thickness of ~1.0 nm (Figure 1). Synthesis and structure of this POM as a mixed K/Li salt, its electrochemistry properties, and also STM studies have been reported previously.[22] Single crystals of $K_{12}Li_{13}[Cu_{20}Cl(OH)_{24}(H_2O)_{12}(P_8W_{48}O_{184})]\cdot 22H_2O$ (KLi−$\{Cu_{20}P_8W_{48}\}$) were carefully weighed and dissolved in water (purified by Milli-Q Direct-Q3 water purification system) at 80 °C with stirring to form solutions of different concentrations. The pale-blue solutions were then dust-freed with Millipore MILLEX-VV 0.1-μm filters (Low Protein Binding Durapore (PVDF)

(13) Wassermann, K.; Dickman, M. H.; Pope, M. T. *Angew. Chem., Int. Ed. Engl.* **1997**, *36*, 1445.
(14) Müller, A.; Krickemeyer, E.; Bögge, H.; Schmidtmann, M.; Peters, F. *Angew. Chem., Int. Ed.* **1998**, *37*, 3360.
(15) Liu, G.; Kistler, M. L.; Li, T.; Bhatt, A.; Liu, T. *J. Clust. Sci.* **2006**, in press.
(16) Kozik, M.; Baker, L. C. W. *J. Am. Chem. Soc.* **1990**, *112*, 7604.
(17) Grigoriev, V. A.; Cheng, D.; Hill, C. L.; Weinstock, I. A. *J. Am. Chem. Soc.* **2001**, *123*, 5292.
(18) Müller, A.; Sarkar, S.; Shah, S. Q. N.; Bögge, H.; Schmidtmann, M.; Sarkar, S.; Kögerler, P.; Hauptfleisch, B.; Trautwein, A. X.; Schünemann, V. *Angew. Chem., Int. Ed.* **1999**, *38*, 3238.
(19) (a) Müller, A.; Das, S. K.; Fedin, V. P.; Krickemeyer, E.; Beugholt, C.; Bögge, H.; Schmidtmann, M.; Hauptfleisch, B. *Z. Anorg. Allg. Chem.* **1999**, *625*, 1187. (b) Müller, A.; Das, S. K.; Krickemeyer, E.; Kuhlmann C. *Inorganic Syntheses*; Shapley, J. R., Ed.; Wiley: New York, 2004; Vol. 34, p 191.
(20) (a) Müller, A.; Koop, M.; Bögge, H.; Schmidtmann, M.; Beugholt, C. *Chem. Commun.* **1998**, 1501. (b) Jiang, C. C.; Wei, Y. G.; Liu, Q.; Zhang, S. W.; Shao, M. C.; Tang, Y. Q. *Chem. Commun.* **1998**, 1937. (c) Müller, A.; Kögerler, P.; Kuhlmann, C. *Chem. Commun.* **1999**, 1347.
(21) Reliable experimental data indicate the blackberry formation in $\{Mo_{176}\}$ solutions. Manuscript in preparation.
(22) (a) Mal, S. S.; Kortz, U. *Angew. Chem., Int. Ed.* **2005**, *44*, 3777. (b) Jabbour, D.; Keita, B.; Nadjo, L.; Kortz, U.; Mal, S. S. *Electrochem. Commun.* **2005**, *7*, 841. (c) Alam, M. S.; Dremov, V.; Müller, P.; Postnikov, A. V.; Mal, S. S.; Hussain, F.; Kortz, U. *Inorg. Chem.* **2006**, *45*, 2866.

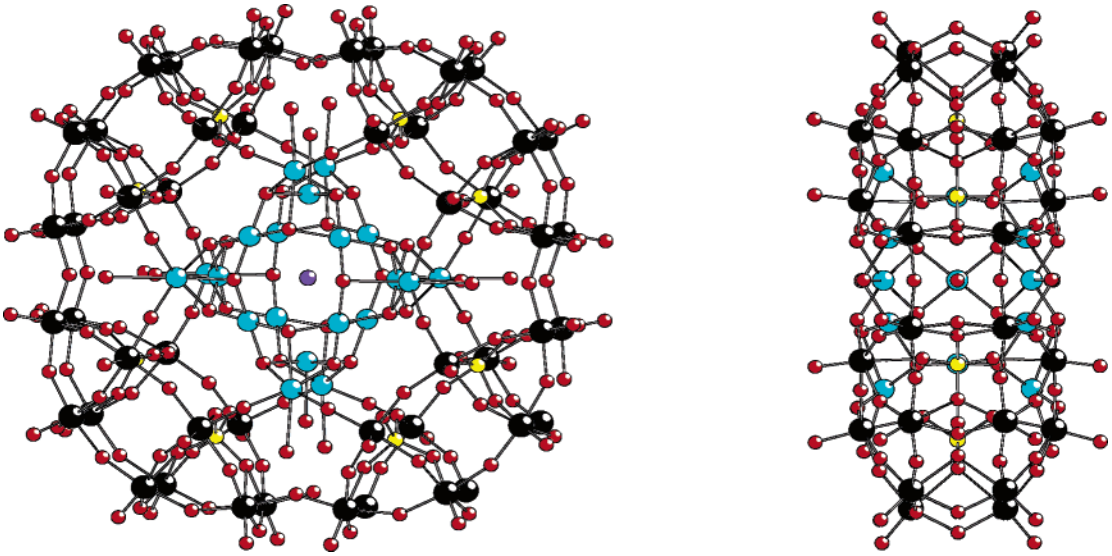

Figure 1. Ball-and-stick representations of $[Cu_{20}Cl(OH)_{24}(H_2O)_{12}(P_8W_{48}O_{184})]^{25-}$ ($\{Cu_{20}P_8W_{48}\}$) macroion viewed along (left) and perpendicular (right) the four-fold symmetry axis (red: O; blue: Cu, black: W; purple: Cl; yellow: P).

membrane) into clean sample cells for dynamic light scattering (DLS), static light scattering (SLS), and zeta potential measurements.

2. Static Light Scattering (SLS) and Dynamic Light Scattering (DLS). The Brookhaven Instruments commercial laser-light scattering spectrometer is capable of performing both SLS and DLS measurements over an angular range of 8−165°. The spectrometer is equipped with two lasers: a JDS Uniphase 50-mW diode-pumped solid-state (DPSS) laser (model μGreen-SLM) operating at 532 nm and a Melles Griot 35-mW He−Ne laser (model 05-LHP-928) operating at 633 nm, and a Brookhaven Instruments BI 9000 AT correlator. The 532-nm laser was used for all the SLS and DLS experiments of current study. The sample chamber was thermostated and could be controlled to within ±0.1 °C. The intensity/intensity−time correlation functions were analyzed by the CONTIN method.[23]

The basis for data analysis of SLS is the Rayleigh−Gans−Debye equation, valid for small, interacting particles in the form:[24]

$$HC/R_{90,532\ nm} = 1/M_w + 2A_2C \tag{1}$$

where $H \equiv 4\pi^2 n_0^2 (dn/dc)^2/N_A\lambda^4$ is an optical parameter with n_0 being the solvent refractive index; N_A, Avogadro's constant; λ, the laser wavelength (532 nm); M_w, weight-average molecular weight of the solutes; A_2, the second virial coefficient; C, solute concentration; and dn/dc, the refractive index increment. R_{90} is the excess Rayleigh ratio of the sample solution at 90°, and it is equal to $R_{Bz,90}(I - I_0)/I_{Bz}(n^2/n_{Bz}^2)$, where $R_{Bz,90}$ is the Rayleigh ratio of benzene at 90°, with a value of 2.0×10^{-5} cm^{-1} at 532 nm;[24] I, I_0, I_{Bz} are the scattered intensities of the sample solution, the solvent, and benzene, respectively and n_{Bz} is the refractive index of benzene. For very dilute solutions such as what we are dealing with here, the $2A_2C$ term is negligible. Because the mass of $\{Cu_{20}P_8W_{48}\}$ supramolecular structures is much larger than that of discrete $\{Cu_{20}P_8W_{48}\}$ clusters, the scattered intensity from the solution is dominantly attributed to the large self-assembled blackberry structures after the self-assembly process has started.

Dynamic light scattering (DLS) measures the intensity/intensity−time correlation function $G^{(2)}(\Gamma)$ by means of a multichannel digital correlator.[25]

$$G^{(2)}(\Gamma) = A(1 + b|g^{(1)}(\Gamma)|^2) \tag{2}$$

where A, b and $|g^{(1)}(\Gamma)|$ are, respectively, the background, a coherence factor, and the normalized electric field time correlation function. The field correlation function was analyzed by the constrained regularized CONTIN[23] method, to yield information on the distribution of the characteristic line width (Γ) from

$$|g^{(1)}(\Gamma)| = \int G(\Gamma)\, e^{-\Gamma\tau}\, d\Gamma \tag{3}$$

The normalized distribution function of the characteristic line width $G(\Gamma)$ so obtained can be used to determine an average apparent diffusion coefficient

$$D_{app} = \Gamma/q^2 \tag{4}$$

where $q \equiv [(4\pi n/\lambda)\sin(\theta/2)]$ is the magnitude of the scattering wave vector. The apparent hydrodynamic radius $R_{h,app}$ is related to D_{app} via the Stokes−Einstein equation:

$$D_{app} = kT/6\pi\eta R_{h,app} \tag{5}$$

where k is the Boltzmann constant and η is the viscosity of solvent at temperature T. From DLS measurements, we can obtain the particle-size distribution in solution from a plot of $\Gamma G(\Gamma)$ versus $R_{h,app}$, with $\Gamma_i G(\Gamma_i)$ being proportional to the scattered intensity of all the i particles having an apparent hydrodynamic radius $R_{h,i}$. The subscript apparent is used to denote DLS measurements performed at finite concentrations when interparticle interactions have been neglected.

During the whole SLS and DLS experiments, the experimental errors in the total scattered intensity and the apparent R_h are about ±2−3%.

3. Zeta Potential Analysis. A Brookhaven Instruments commercial *ZetaPALS* analyzer was used to measure the zeta potential and the mobility of the particles in sample solutions. The analyzer was equipped with a 35-mW solid-state laser operating at 660 nm. The sample chamber was thermostated in a range of 6−74 °C and could be controlled to within ±0.1 °C. According to the instrument design, particles with diameters from 10 nm to 30 μm (depending on particle density) and zeta potential ranging from −150 to +150 mV could be measured, and the data accuracy and repeatability were both ±2% for dust free samples.

The mobility of particles is related to the their zeta potential value by:

$$\mu = \xi\epsilon f(\kappa a,\xi)/\eta \tag{6}$$

(23) Provencher, S. W. *Biophys. J.* **1976**, *16*, 29.
(24) Hiemenz, P.; Rajagopalan, R. *Principles of Colloid and Surface Chemistry*; Marcel Dekker: New York, 1997; Chapter 5.
(25) Chu, B. *Laser Light Scattering*, 2nd ed.; Academic Press: New York, 1991.

where μ, ξ, ϵ, η, and the factor $f(\kappa a,\xi)$ are the electrophoretic mobility of the particles, zeta potential, the solvent dielectric constant, the solvent viscosity, and a model-dependent function with Debye parameter κ being the reciprocal of double layer thickness and a being the radius of the kinetic unit, respectively. Conventional laser Doppler electrophoresis is limited to the mobility of 0.5×10^{-8} m^2 s V^{-1} and cannot readily be used to measure lower mobility due to the limitation in the resolution of frequency and the background drifts in the sample due to thermal fluctuations. Unfortunately, the mobilities of POM blackberries are usually much lower than 0.5×10^{-8} m^2 s V^{-1}. Therefore, a new method other than direct frequency analysis is necessary to measure the Doppler shift. If the Doppler signal is compared to a reference signal corresponding to stationary particles using phase quadrature, any small change in frequency eventually gives rise to a change in phase between the signals. This phase change, $Q(t)$, can be related to the Doppler shift and hence the electrophoretic mobility by measuring a phase $Q(t)$ in the scattered light field at scattering vector q which changes due the movement of particles with mobility μ in an electric field $E(t)$. Given that the scattered light has amplitude of A,

$$\langle Q(t) - Q(0)\rangle = \langle A\rangle q\mu \int_0^t E(t')\mathrm{d}t' \qquad (7)$$

For the case of a sinusoidal field the integral gives the following result,

$$\langle Q(t) - Q(0)\rangle = \langle A\rangle q\mu\{\cos(\phi) - \cos(\omega t + \phi)\}/\omega \qquad (8)$$

where ω is the frequency of the applied electric field. The *ZetaPALS* hardware incorporates a digital signal processor which can extract $Q(t)$ directly from the Doppler signal. Thus, the mobility and zeta potential can be calculated.

4. Scanning Electron Microscopy (SEM). A FEI/Philips XL-30 ESEM was used for SEM measurements in high-vacuum mode. Sample solutions were dropped on the surface of SPI aluminum specimen mounts and dried in air prior to measurements.

Results and Discussions

Monitoring the Slow Self-Association of {$Cu_{20}P_8W_{48}$} Supramolecular Structures in Dilute Aqueous Solutions by SLS and DLS. A series of dilute {$Cu_{20}P_8W_{48}$} aqueous solutions at different concentrations (up to 0.5 mg/mL) were prepared for SLS and DLS studies. Freshly prepared {$Cu_{20}P_8W_{48}$} solutions showed very weak scattered intensities in SLS measurements, indicating that there were nearly no large structures in solution, i.e., the {$Cu_{20}P_8W_{48}$} macroions basically existed as discrete ions distributed homogeneously in solution. This is very similar to common, simple electrolyte solutions. The solutions were kept at 50 °C and monitored by SLS frequently. The scattered intensity from the SLS measurements did not show any change during the first several days, but a sudden increase was then observed for all solutions. For example, for the 0.5 mg/mL {$Cu_{20}P_8W_{48}$} solution, the scattered intensity suddenly increased on the 8th day and continued to increase in the following days, suggesting the formation of large structures in solution, as shown in Figure 2. This type of delay at the beginning of the self-assembly process, possibly related to the kinetic process of the supramolecular structure formation in solution, has also been observed in the blackberry formation of other types of POM macroions. The length of this delay period seems to depend not only on the macroionic structure, but also on temperature, solution pH ionic strength, and solvent composition.

Similar to our previously reported {$Mo_{72}Fe_{30}$} aqueous solutions, after the "delay" period, the increment of scattered intensity was continuous but slow, especially at lower temperatures, suggesting a very slow self-assembly process due to a high energy barrier.[10] At 50 °C, the scattered intensity from the 0.5 mg/mL {$Cu_{20}P_8W_{48}$} solution continued to grow within the next 40 days, until finally becoming stable, suggesting that equilibrium between discrete {$Cu_{20}P_8W_{48}$} macroions and large supramolecular structures had been reached (Figure 2). Studies on {$Cu_{20}P_8W_{48}$} solutions at lower concentrations show very similar scattered intensity−time curves.

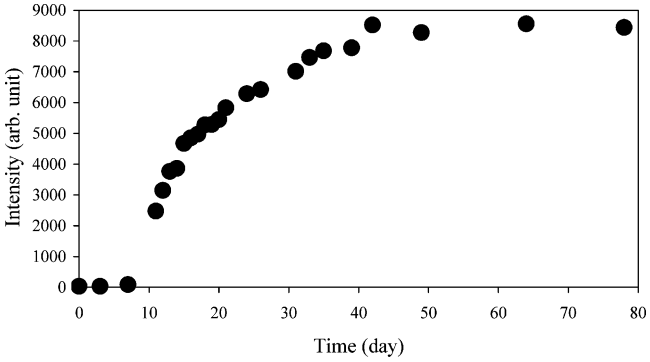

Figure 2. Growth of scattered light intensity with time from a 0.5 mg/mL {$Cu_{20}P_8W_{48}$} solution at 50 °C.

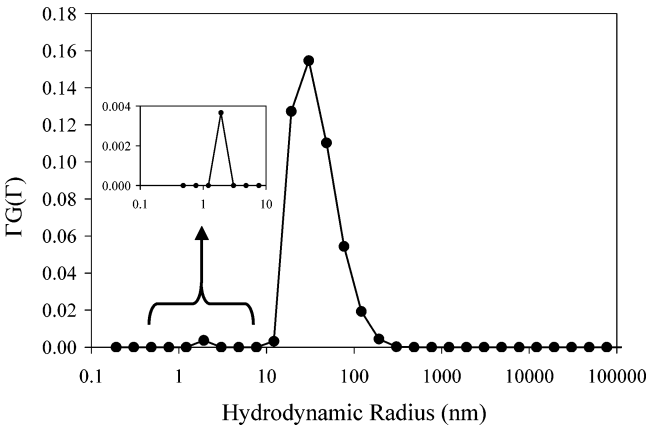

Figure 3. CONTIN analysis of a DLS study on a 0.5 mg/mL {$Cu_{20}P_8W_{48}$} aqueous solution at 90° scattering angle on the 11th day. (Insert)Peak attributed to free {$Cu_{20}P_8W_{48}$} macroions.

The slow supramolecular structure formation in {$Cu_{20}P_8W_{48}$} solutions can also be monitored by the DLS technique. A typical CONTIN[23] analysis from a DLS study on a 0.5 mg/mL {$Cu_{20}P_8W_{48}$} solution on the 11th day of the experiment at scattering angle of 90° is shown in Figure 3, where two different modes can be identified, corresponding to two different types of species in solution: the peak at $R_{h,90} \approx 1.9$ nm should be attributed to discrete {$Cu_{20}P_8W_{48}$} macroions (Figure 3, insert) and the peak at $R_{h,90} = 30.2$ nm should be attributed to large supramolecular structures assembled by {$Cu_{20}P_8W_{48}$} macroions. Even on day 11 (3 days after the supramolecular structure formation started), the peak due to the supramolecular structures was already dominant, and the peak corresponding to discrete ions could barely be identified. This result does not suggest that most discrete macroions have formed supramolecular structures at this moment. Equation 1 for SLS can be simplified to:

$$I_i \propto C_i \cdot M_{w,i} \qquad (9)$$

with I_i being the scattered intensity contributed from species I

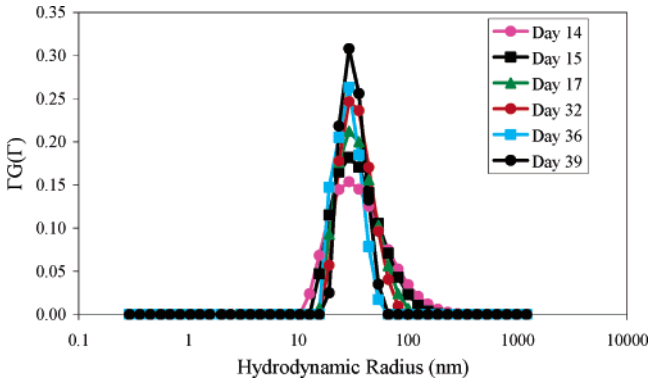

Figure 4. CONTIN analysis of a DLS study on a 0.5 mg/mL $\{Cu_{20}P_8W_{48}\}$ solution maintained at 50 °C and 90° scattering angle at different times. Starting from day 14, the small peak attributed to free macroions could not be detected by CONTIN analysis, due to the fact that the scattered light was dominantly from large blackberry-type structures.

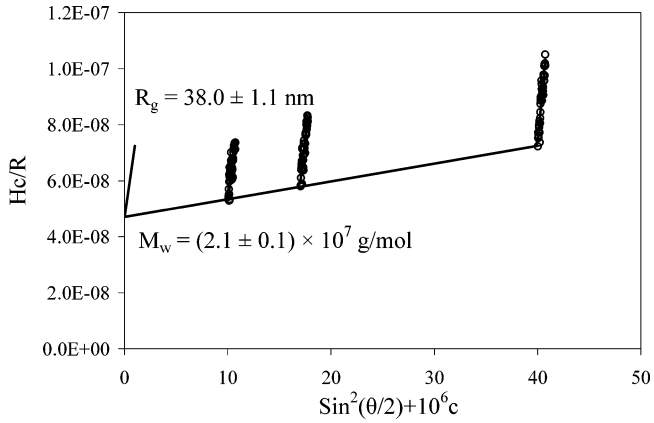

Figure 5. Zimm plot based on SLS measurements of 0.010, 0.017, and 0.039 mg/mL $\{Cu_{20}P_8W_{48}\}$ solutions. The measurement was performed after the solution had reached equilibrium. The average radius of gyration (R_g) and the weight-average molecular mass (M_w) of blackberry-type structures can be determined. The latter value was calculated on the basis of the assumption that all $\{Cu_{20}P_8W_{48}\}$ macroions have formed blackberry-type structures. This assumption might introduce some error, leading to a lower estimated M_w.

and C_i having the unit of mg/mL. It is obvious that large particles scatter the incident beam more strongerly than small particles due to their much larger mass, i.e., a small number of large particles can scatter incident light more strongly than many more small particles. The relative peak areas in Figure 3 reflect the contributions to the total scattered intensities from two types of species. Because the size of the supramolecular structures is much larger than that of the discrete $\{Cu_{20}P_8W_{48}\}$ macroions, the contribution to the scattered intensity from large structures is dominant. The small peak due to discrete macroions in Figure 3 became even smaller and smaller with time, and finally could not be identified from CONTIN analysis. At the same time, the large peak became more and more dominant with time (Figure 4), indicating a continuous formation of large structures. Interestingly, the measured average R_h of the supramolecular structures does not show obvious changes over time with the macroionic concentration between 0.03 and ~0.5 mg/mL.

Characterization of the Self-Assembled $\{Cu_{20}P_8W_{48}\}$ Supramolecular Structures. After about 6 weeks, the scattered intensity from macroionic solutions stopped increasing and kept roughly steady thereafter, showing that the self-assembly had reached equilibrium. Many detailed SLS and DLS studies can be carried out at this stage to obtain structural information on the $\{Cu_{20}P_8W_{48}\}$ self-assembled structures. The accurate, average hydrodynamic radius of the supramolecular structures can be determined by extrapolating R_h values at different scattering angles to zero scattering angle ($R_{h,0}$). DLS measurements showed a weak angular dependence of the R_h value, suggesting a predominantly spherical shape of the large assemblies. Extrapolating the R_h values to zero scattering angle and zero concentration results in $R_{h,0} = 38.1 \pm 1.0$ nm.

The SLS data, analyzed by Zimm plot (Figure 5), shows that the supramolecular structures have a weight-average molecular weight (M_w) of ~$(2.1 \pm 0.1) \times 10^7$ g/mol, and an average radius of gyration (R_g) of 38.0 ± 1.1 nm. It is noteworthy that the R_g and $R_{h,0}$ values of the spherical objects (evidence from SEM images in next section, as well as the evidence from the weak angular dependence of R_h values) are roughly the same. For a solid spherical particle, $R_g = 0.77R_{h,0}$,[26] i.e., $R_g \approx 29$ nm for a sphere with $R_{h,0} \approx 38$ nm, much smaller than the experimental value. The ratio of $R_g/R_{h,0}$ will increase if more mass distributes closer to the surface in a sphere. If the spherical objects have all their mass distributed on the surface, then $R_g/R_{h,0} = 1$, which is the current case. This is a typical model for a vesicle-like structure. Therefore, the large aggregates formed in $\{Cu_{20}P_8W_{48}\}$ solutions are also vesicle-like blackberry-type structures, as we have shown previously.[4−12] Further evidence comes from the M_w of the aggregates. The M_w of $(2.1 \pm 0.1) \times 10^7$ g/mol is equivalent to ~1522 ± 76 $\{Cu_{20}P_8W_{48}\}$ macroions, which is very short of forming 38-nm-radius solid spheres. In KLi−$\{Cu_{20}P_8W_{48}\}$ single crystals,[22] there are two $\{Cu_{20}P_8W_{48}\}$ clusters in each 15.2 nm^3 unit cell. Therefore, if the aggregates were solid $\{Cu_{20}P_8W_{48}\}$ nanocrystals, each spherical aggregate would contain ~30,000 single clusters. This large discrepancy strongly suggests that the aggregates cannot be solid. Interestingly, distributing 1522 $\{Cu_{20}P_8W_{48}\}$ macroions on a 38-nm-radius sphere surface results in an average center-to-center distance of 3.7 ± 0.2 nm between adjacent macroions, and an average intercluster distance of 1.7 ± 0.2 nm. This distance is too large to be acceptable, although it is reasonable to see that the macroanions do not touch each other on the surface of blackberry-type structures.[7] The very large, unreasonable intermacroionic distance should be due to the fact that the SLS studies underestimated the mass of blackberries because we have assumed that all macroions in solution have formed blackberry-type structures. However, in the current case there might still be a large number of discrete macroions in equilibrium with "blackberries" in solution, i.e., the actual concentration of blackberry-type structures in solution is lower than what we assumed. As a result, the number of macroions in each blackberry-type structure would be underestimated, leading to an overestimated intermacroion distance (but this does not affect the R_g). Previously, we have found that the intercluster distance should be smaller than 1 nm.[7] Figure 6 is a cartoon picture showing $\{Cu_{20}P_8W_{48}\}$ blackberry-type structures.

The $\{Cu_{20}P_8W_{48}\}$ blackberry-type structure solutions are very stable. For the solutions that have already reached the equilibrium, keeping them at 50 °C for months does not result in obvious changes in scattered intensity as determined from SLS measurements, and there is no change in the average $R_{h,0}$'s of the supramolecular structures as determined by DLS measure-

(26) Tanford, C. *Physical Chemistry of Macromolecules*; John Wiley and Sons: New York and London, 1961.

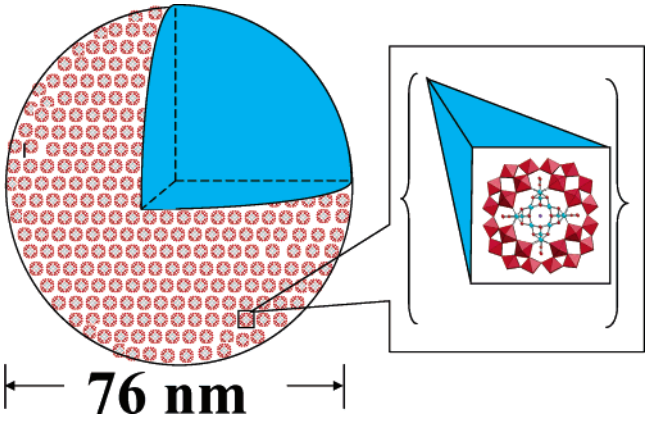

Figure 6. Cartoon showing $\{Cu_{20}P_8W_{48}\}$ blackberry-type structure based on SLS and DLS measurements.

ments. Dilution also does not change the size of blackberry-type structures. As we described earlier,[10] the blackberry state is a free-energy-favored state that is more stable than the homogeneous distribution of macroions in solution.

The above SLS and DLS studies were based on $\{Cu_{20}P_8W_{48}\}$ solutions kept at 50 °C. Other solutions kept at 25, 30, and 40 °C also gave similar results. The major difference is that the blackberry-type structure formation became slower at a lower temperature.

SEM Studies on the Morphology of $\{Cu_{20}P_8W_{48}\}$ Blackberries. The weak angular dependence of the R_h values for the $\{Cu_{20}P_8W_{48}\}$ blackberry-type structures suggests that they have a relatively isotropic morphology. SEM studies were performed to further clarify this point. SEM measurements show that the substrate is covered by many spherical objects, quite uniform in size, with an average radius of ~40 nm (Figure 7a). These objects should be attributed to $\{Cu_{20}P_8W_{48}\}$ blackberry-type structures, and their measured average radius is consistent with light-scattering studies ($R_{h,0} \approx 38$ nm). It should be mentioned that the SEM image was taken on a dried sample on a metal surface on high vacuum. This was a different environment from the dilute solution state and might lead to deformation of the blackberry-type structures if considering their soft and single-layer features. For comparison, an SEM image of $\{Cu_{20}P_8W_{48}\}$ microcrystals is shown in Figure 7b. The obvious morphology differences between the two images clearly shows that the large structures formed in solution are not $\{Cu_{20}P_8W_{48}\}$ microcrystals, but rather blackberry-type structures. The latter form clear, thermodynamically stable solutions, while microcrystals continuously grow until they precipitate from solution (crystallization).

The Mechanism of Blackberry-Type Structure Formation. Monitoring the $\{Cu_{20}P_8W_{48}\}$ solutions continuously with SLS and DLS can provide important information regarding the mechanism of blackberry-type structure formation. There are two possible routes to explain the slow formation of blackberry-type structures, as shown in Figure 8. In both cases, when the single crystals of KLi−$\{Cu_{20}P_8W_{48}\}$ are just dissolved in solution, the $\{Cu_{20}P_8W_{48}\}$ clusters exist as discrete macroanions. In scenario one, a few $\{Cu_{20}P_8W_{48}\}$ clusters slowly nucleate together after overcoming a major energy barrier, and then quickly form a blackberry-type structure with a radius of ~38 nm, the favored size for $\{Cu_{20}P_8W_{48}\}$ blackberry-type structures at the current conditions. The blackberry-type structure does not further nucleate with other macroions or blackberry-type structures to grow larger. On the other hand, the remaining macroions will try to form another blackberry slowly, which will again stop growing when its radius is around 38 nm. At the end, the solution contains many blackberry-type structures relatively uniform in size. In other words, the speed of blackberry-type structure formation is controlled by the high activation energy barrier between the two states, and not

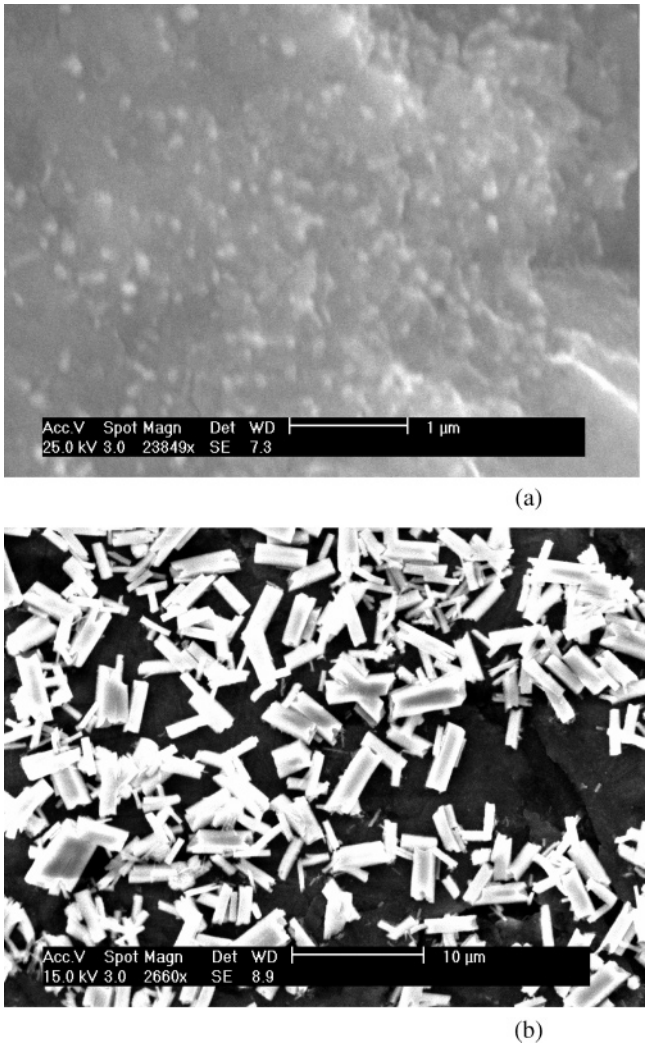

Figure 7. SEM studies on $\{Cu_{20}P_8W_{48}\}$ systems. (a) Sample was prepared from a homogeneous aqueous $\{Cu_{20}P_8W_{48}\}$ aqueous solution drying on a SPI aluminum specimen mount surface. Spherical and uniform structures with average radius ~40 nm can be seen, which are attributed to blackberry-type structures formed in solution. (b) Microcrystals obtained from precipitation/crystallization of a saturated $\{Cu_{20}P_8W_{48}\}$ solution, showing typical single-crystal features.

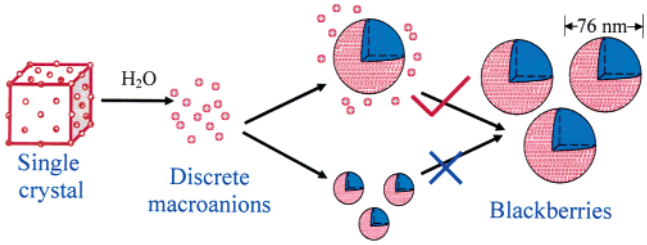

Figure 8. Possible mechanisms of $\{Cu_{20}P_8W_{48}\}$ blackberry formation in dilute aqueous solution. On the basis of SLS and DLS results, the upper mechanism has been proven to be correct, while the bottom mechanism can be ruled out.

controlled by the diffusion of macroions in solution. In scenario two, many small $\{Cu_{20}P_8W_{48}\}$ blackberry-type structures are formed in solution quickly. However, the growth of each individual blackberry-type structure is very slow, which could be due to the limited availability of macroions around those small associations. While we cannot distinguish these two mechanisms from the change of scattered intensity, DLS measurements can offer a satisfying answer. As shown in Figure 4, the average R_h of the blackberry-type structures does not show an evident change with time, i.e., during the process of blackberry-type structure formation. This is strong evidence for the first scenario (Figure 8). This can be further confirmed by the fact that the blackberry-type structure formation becomes much faster at higher temperatures because the macroions with higher kinetic energy can overcome the energy barrier more easily. On the other hand, increasing macroionic concentration does not speed up the blackberry-type structure formation significantly, and the blackberry-type structures also do not grow larger. These observations suggest that scenario two is unlikely.

After reaching equilibrium, the size of the blackberry-type structures remains almost unchanged with time, showing features of a system at equilibrium. Continuous growth of blackberry-type structures to larger size and consequent precipitation have not been observed for any type of POM solutions, including the current one, without changing the external conditions (e.g. adding large amounts of electrolyte).

Electrophoretic Properties of $\{Cu_{20}P_8W_{48}\}$ Blackberry-Type Structures. An important aspect of the self-assembly of macroions is the effect of counterions. Previously we speculated that the counterion-mediated attraction between macroions might be important for the blackberry-type structure formation, after we concluded that the van der Waals forces and major chemical interactions (such as metal−oxygen−metal bonds) are not the major attractive forces between macroions.[9] This is also a major difference between hydrophilic macroions and hydrophobic colloidal suspensions. To understand the role of counterions in dilute macroionic solutions, it is important to study the state of counterions, i.e., whether they are still "free" cations in the presence of large macroanions. Considering that there is no buffer electrolyte in solution, and the macroions are the only type of anions, simple conductivity measurements can be used for this study. Recently, we observed the counterion association phenomenon for dilute $\{Mo_{132}\}$ and $\{W_{148}\}$ macroionic solutions containing discrete macroions.[21] In those solutions, only a fraction of the cations (~80%, depending on the ionic concentration) contributes to the solution conductance as free ions, leading to a much lower total solution conductance than the calculated value (assuming all cations are free). The counterion association effect becomes more significant at higher ionic concentrations. Such an association effect is due to the disparity in size and number of charges between POM macroions and the much smaller counterions.[21]

However, the electrophoretic properties of blackberry-type structures have not been studied. Such a study is important to understand the state of counterions in blackberry-type structure solutions and the role of counterions in the formation of blackberry-type structures. Here we used zeta potential analysis to study the state of counterions in blackberry-type structure solutions by measuring their electrophoretic mobility. Zeta potential analysis is widely used to determine the zeta potential

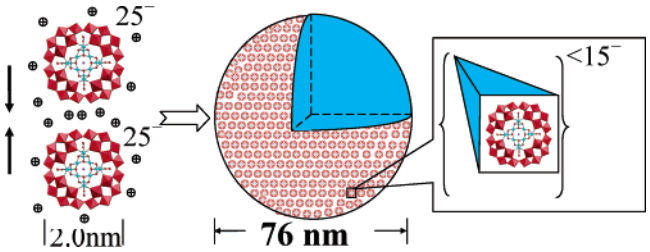

Figure 9. In the blackberry-type structures, each $\{Cu_{20}P_8W_{48}\}$ cluster carries less than 15 negative charges on average. On the other hand, in single crystals each cluster carries 25 charges. This difference clearly indicates that some small cations must be closely associated with, or incorporated into, the large blackberry-type structures. The cations play an important stabilizing role in the assembly of the blackberry-type structures by providing an attractive force.

values of colloidal systems by measuring the mobility of colloid particles in an external electric field. Different approximations are needed for different types of systems (depending on the κa values). Compared to traditional colloidal systems, the POM macroions have much smaller sizes and higher charge densities. Consequently, the κa values for macroions are very small, and within the Hückel limit.

According to its chemical formula, each $\{Cu_{20}P_8W_{48}\}$ macroion carries 25 negative charges, balanced by 12 K^+ and 13 Li^+. The aqueous $\{Cu_{20}P_8W_{48}\}$ solutions have pH values very close to 7 (between 6.5 and 7.0), indicating that there is almost no H^+ or OH^- released from clusters into solution. For a 0.04 mg/mL $\{Cu_{20}P_8W_{48}\}$ solution, the mean mobility of the blackberry-type structures was determined by zeta potential analysis as $-(0.59 \pm 0.05) \times 10^{-6}$ cm^2 V^{-1} s^{-1} after 10 runs (each run has 50 cycles of measurements). The ion mobility is related to the charge on particles via the Hückel equation:

$$\mu_0 = q/6\pi\eta r \qquad (10)$$

with μ_0, η, q, and r being the absolute mobility of particles at zero buffer ionic strength, the solvent viscosity, the charge on particles, and the particle radius, respectively.[27] In our current case, because the solution contains no buffer ions, the measured mobility is μ_0. Consequently, the average charge on each $\{Cu_{20}P_8W_{48}\}$ blackberry-type structure is estimated as $-(2.3 \pm 0.2) \times 10^4$, with the negative sign denoting negative charges. As determined by SLS, each blackberry-type structure is, on average, composed of ~1522 ± 76 $\{Cu_{20}P_8W_{48}\}$ macroions; thus, the charge on each $\{Cu_{20}P_8W_{48}\}$ macroion in blackberry-type structures is calculated as -15 ± 1. Considering that we might have underestimated the mass of the blackberry-type structures in SLS measurements, the actual number of macroions in each blackberry-type structure could be higher. Therefore, the actual number of charges on each macroion could even be smaller than 15. In any case, the number is significantly smaller than 25, indicating that some counterions must be closely associated with, or even incorporated into, the blackberry-type structures (Figure 9). The presence of these associated counterions may arise prior to or after the blackberry-type structure formation. Before the blackberry-type structure formation, some counterions might already be associated with the $\{Cu_{20}P_8W_{48}\}$ macroions such as seen for the cases of $\{Mo_{132}\}$ and $\{W_{148}\}$ solutions,[21] which can shield the negative charges on the macroions partially and allow for a counterion-mediated attrac-

(27) Roy, K. I.; Lucy, C. A. *Electrophoresis* **2003**, *24*, 370.

tion between them. Some of these associated cations might be released into solution during the blackberry-type structure formation, leading to an increase in entropy which helps to decrease the free energy of blackberry-type structures. After the blackberry-type structure formation, some counterions are attracted to and associated with large blackberries. Many counterions being closely associated with blackberry-type structures is, of course, not direct evidence to show that the counterions provide a major attractive force responsible for the self-assembly of macroions. However, this is a realistic scenario, especially when considering that the macroions alone cannot be in close proximity on the blackberry-type structure surface due to electrostatic repulsion.[7]

Summary

In summary, we have discovered that the wheel-shaped, copper-containing, tungstophosphate $\{Cu_{20}P_8W_{48}\}$ macroions self-assemble into blackberry-type structures. These results indicate that this novel type of self-assembly is a relatively universal phenomenon for hydrophilic macroions and certainly not limited to large, Mo-containing POM clusters. We believe that there is no significant covalent bonding (such as metal−oxygen−metal) taking place during the blackberry-type structure formation. Therefore, the type of addenda atom (e.g., W, Mo) in a POM does not appear to significantly influence its supramolecular solution chemistry. Instead, the size and charge density of the macroions, the nature of the charges on clusters (localized or delocalized), and the complex electrostatic interaction with counterions seem to be very important parameters.

By now, blackberry-type structure formation has been demonstrated for quite a few types of nanometer-scaled POM species, and $\{Cu_{20}P_8W_{48}\}$ is the smallest of them. As the disparity between macroanions and small cations might be important (responsible for the counterion association effect), it is interesting for both theorists and experimentalists to explore at what size regular, simple ions start to show properties of macroions. The fact that $\{Cu_{20}P_8W_{48}\}$ macroions can form blackberry-type structures enables us to move one step closer toward identifying the transition point between simple ions and macroions.

Furthermore, the current study represents the first attempt to understand the electrophoretic properties of blackberry-type structures, a type of charged supramolecular structure, in dilute aqueous solutions. The mobility of blackberry-type structures measured from zeta-potential analysis supports the idea that alkali counterions are associated and/or incorporated into blackberry-type structures and possibly provide a crucial attractive force which compensates the repulsive interactions between $\{Cu_{20}P_8W_{48}\}$ macroanions and therefore facilitates blackberry-type structure formation.

Acknowledgment. T.L. gratefully acknowledges support from the National Science Foundation (NSF-CHE0545983), Lehigh University (startup fund and FRG), and NSFC (20428101). U.K. acknowledges support from the International University Bremen and the German Science Foundation (KO 2288/3-1).

JA0610840